

Development of an Iron-Based Hardfacing Material Reinforced with Fe-(TiW)C Composite Powder

E.O. CORREA, N.G. ALCANTARA, D.G. TECCO, and R.V. KUMAR

The objective of this work is to investigate the correlation of microstructure with wear resistance in a hardfacing material reinforced with Fe-(TiW)C composite powder particles. This material was designed for cladding components subjected to highly abrasive conditions and was deposited on a low-carbon steel substrate by open arc welding. The theoretical and experimental work undertaken includes solidification study, microstructural characterization, and abrasive wear testing. Microstructural analysis of the hardfaced top layer of the alloy showed the presence of TiWC carbide particles and TiNbC carbides randomly distributed in a eutectic mixture matrix γ/M_7C_3 containing primary austenite dendrites. Microstructural examinations also showed that hard and fine spherulitic carbides, in which a Ti-rich MC carbide core was encircled by MC carbide enriched with Nb and W, were homogeneously distributed in the matrix. The energy-dispersive spectroscopy (EDS) mapping of spherulitic carbides showed that the any added Nb replaced a significant part of W in the Fe-(TiW)C powder, and W preferentially partitioned into other carbides and matrix during solidification. Abrasion test results showed that the preceding carbides improve the wear resistance of the hardfacing material in comparison with conventional Fe-Cr-C and Fe-Cr-C-Nb alloys, especially under high stress conditions.

DOI: 10.1007/s11661-007-9141-6

© The Minerals, Metals & Materials Society and ASM International 2007

I. INTRODUCTION

REDUCTION of wear is achieved by applying a wear-resistant surface onto a cheaper and a tougher core material. Many examples of hardfacing materials tend to be alloys containing hard carbides. It may be possible to incorporate hard carbide ceramic particles into a metal matrix to produce metal matrix composites (MMCs) that can withstand high abrasive wear environments. In the last decade, much attention has been paid to the production of MMCs by the “*in-situ*” synthesis technique, whereby carbide reinforcements are produced *in situ* in a metal matrix during melting and solidification. The advantage of obtaining composites using this technique is that it eliminates interface incompatibility between the matrix and the reinforcing particles via precipitation by nucleating and growing thermodynamically stable carbides with good bonding with the metal matrix. The first composite powder synthesized using the *in-situ* synthesis technique was based on TiC in a ferrous matrix.^[1,2] However, it was noted that due to the substantial difference in density between TiC

(4.25 g cm^{-3}) and iron melt (7.8 g cm^{-3}), the relatively light TiC particles tended to float up during solidification, resulting in their segregation in the cast composites. (TiW)C-based powders were found therefore to be a better choice for reinforcements synthesized *in situ* in an iron melt, because their density at 9.1 g cm^{-3} is higher than that of TiC and of similar order as that of iron and, they have no tendency to float out of the iron melt.^[3]

Although conventional metallic Fe-Ti and Fe-Nb powders are often added to Fe-Cr-C type hardfacing alloys in order to obtain very hard and fine MC carbides in the microstructure and, consequently, to improve significantly the wear resistance of these alloys, little has been published regarding the addition of the Fe-(TiW)C composite powder as reinforcement in Fe-Cr-C hardfacing alloys. In many applications, where excellent wear resistance and sufficient impact resistance are required, hardfacing alloys modified with these composite particles may be advantageous as the presence of these composite powders in the microstructure of hardfacing alloys may improve their wear resistance without greatly sacrificing toughness.

In the present study therefore, a hardfacing alloy reinforced with complex carbide composite was investigated. The microstructure of the hardfacing alloy was analyzed and its hardness and wear resistance were evaluated. The data were compared with those for conventional Fe-Cr-C and Fe-Cr-C-Nb type hardfacing alloys with a view to identify the mechanism involved in achieving improved wear resistance properties.

E.O. CORREA, Researcher, is with the Department of Materials Science and Metallurgy, University of Cambridge, is with the Universidade Federal de Itajubá, Minas Gerais, Brazil. N.G. ALCANTARA, Professor, is with the Universidade Federal de São Carlos, São Paulo, Brazil. D.G. TECCO, Director, is with the Welding Alloys Ltd., Fowlmere, Royston, Herts, United Kingdom. R.V. KUMAR, Senior Lecturer, is with the Department of Materials Science and Metallurgy, University of Cambridge, Cambridge, United Kingdom. Contact e-mail: rvk10@cam.ac.uk

Manuscript submitted May 17, 2006.

Article published online May 25, 2007.

II. EXPERIMENTAL

A. Manufacture of Cladding Electrode

The complex carbide composite powder used in this study is based on metallic Fe and mixed carbides of Ti and W. The composite, represented as Fe-(TiW)C, which was supplied by London and Scandinavian Metallurgical Co., Ltd. (London), was manufactured using a self-propagating high-temperature synthesis method.^[5,6] The chemical composition is shown in Table I. According to the specification, a maximum 2 wt pct of the carbon may be present as free carbon.^[7] From the composition, the molar ratio of Fe:TiC:WC can be calculated to be 2:3:1. According to results in the literature, W exists within a mixed $Ti_{0.5}W_{0.5}C$ phase. Accordingly, the composite powder can be chemically represented as Fe-TiC- $Ti_{0.5}W_{0.5}C$ with the three phases present in equal molar ratio. A small proportion of Ti and W can dissolve in the Fe matrix, resulting in the presence of some unreacted free C.

The Fe-(TiW)C powder was extremely fine in the micron-submicron range; it was difficult to handle; and metallic powders of Fe-Cr, Fe-Mn, Fe-Nb, and Fe-Si were included to help the fabrication of the electrode. Table II lists the weight fractions of the various powders charged into the electrode. Graphite and stainless steel was added to adjust the amount of C, Fe, and Cr to be required in the weld metal deposit. After mixing, the powder mixture was inserted into a metallic sheath formed rounded to a semicircular shape. It was then closed off into a tubular shape and was roll formed into the selected diameter of 2.8 mm, which served as the welding electrode. After mixing, the powder mixture was inserted into a metallic sheath formed in a U shape. It was then closed in an O shape and was roll formed into the desired diameter of 2.8 mm to manufacture the electrode. Table II lists the weight fractions of the various powders charged into the electrode.

B. Study of Alloy Solidification

In this work, hardfacing on the surface of steel was done, by using open arc welding with a tubular welding electrode. Due to the high cooling rates involved in the welding process, the weld metal microstructure obtained

is in a thermodynamic nonequilibrium condition. In addition, heat treatments, when applied in the weld metal, are not severe enough to enable equilibrium conditions to be achieved. The fact that nonequilibrium solidification occurs therefore had to be considered to ensure that realistic solidification models were obtained.

A useful alloy solidification model, which takes into account this nonequilibrium condition, can be obtained using the Scheil simulation module of MT-DATA in conjunction with the *plus* and *sub-sgte* databases.^[4] In the Scheil model, it is assumed that no diffusion occurs in the solid, while there is a perfect mixing in the liquid during solidification. Microstructural characterization (including data obtained from energy-dispersive spectroscopy (EDS) and image analysis) was used to validate the solidification model of the alloy.

C. Open-Arc Welding

Open-arc welding is a cost-effective automatic welding technique particularly suited to hardfacing applications. This technique has the merits of dispensing flux and shield gas as well as being able to use a large electric current and enabling rapid welding.

Hardfacing was done on a mild steel plate of 40-mm thickness under the conditions shown in Table III. The weld deposit consisted of eight layers overlapped (approximately 18-mm height) and was processed by depositing several beads. It was possible with this procedure to eliminate the effect of dilution upon the microstructure of the hardfaced layer and reproduce realistically the conditions of cladding in large components (for example, rolls and tables) used in cement and mineral industries.

The chemical composition of the undiluted top layer of the hardfaced alloys, obtained by optical emission spectrometry, after the welding process, is shown in Table IV. The alloy designated HCO is a conventional high-chromium white iron containing primary and

Table I. Chemical Composition of Composite Powder Used, Weight Used

Composite Powder	Fe	W	Ti	C
Fe-(TiW)C	balance	34.8	29.6	10.3

Table II. Weight Fraction of the Powders Included Inside of the Hardfacing Electrode

Powder						
Fe-Cr	Fe-Nb	Fe-Mn	Fe-Si	Fe-(TiW)C	Graphite Fine + Coarse	Stainless Steel 430 Wire Peels 16 × 0.3 mm
9.6	9.5	1.8	1.4	24.0	2.50	51

Table III. Welding Conditions

Arc voltage	28 to 31 V (DC)
Welding current	450 to 500 A
Electrode polarity	positive
Wire feeding rate	4.5 m/min
Traveling speed	1.5 m/min
Preheating	no
Electrode angle	10 deg to plate surface
Electrode extension	30 mm
Bead step over	6 mm
Bead type	stringer (no oscillation)

Table IV. Composition of the Top Layer of Alloys in As-Welded Condition (Eight Layer Deposits), Weight Percent (Balance Fe)

Hardfacing electrode	C	Si	Mn	Cr	W	Nb	Ti	V
HCO	4.85	0.8	1.1	24.5	—	—	—	—
CNO	4.80	0.9	0.7	21.6	—	6.4	—	—
700	5.50	1.15	1.25	15.30	7.80	7.6	4.20	0.20

eutectic $(Fe,Cr)_7C_3$ carbides. The alloy CNO is a high-chromium white iron containing Nb, and its microstructure consists of uniformly distributed fines NbC carbides and primary M_7C_3 carbides in the eutectic mixture matrix γ/M_7C_3 . The alloy designated 700 is the hardfacing deposit using the electrode, which included the Fe-(TiW)C composite powder, as described in Table II.

D. Microstructural Characterization and Hardness Test

The hardfaced specimens were sectioned transverse to the surface, then polished and etched with Villela reagent. Microstructural examinations of the specimens were carried out using standard optical microscopy and scanning electron microscopy. X-ray diffraction and EDS facilities available on a scanning electron microscope (SEM) enabled analysis of individual phases present in the alloy and their chemical compositions to be estimated. Procedures involving heavy etching of specimens in a $CuCl_2$ -HCl mixture were used to perform quantitative analysis of phases. Image processing and an image analysis computer program were subsequently used to determine the volume fraction of phases. Some abrasion test specimens were selected to examine abraded surfaces in the SEM, in an attempt to provide a better understanding of wear mechanism.

The overall bulk hardness of the hardfaced layer and microhardness of the matrix and individual phases were measured using a Vickers hardness tester under 30 kg and 100 g loads, respectively.

E. Wear Tests

Low stress abrasive wear-resistance tests were performed on the wear-resistant part using a dry sand rubber wheel abrasive wear tester (RWAT), in accordance with ASTM G65-01-Procedure A.^[8] The RWAT test specimens with dimensions $25 \times 75 \times 16$ mm were worn in contact with sand between rubber wheel under a testing load of 13.5 kg. The average diameter of the dry sand grains was 0.2 mm, and the total wear distance was 4.5 km. Specimens were weighed before and after the test and mass losses were converted into volume losses.

High stress abrasive tests using the pin-on-disc method were carried out on 6-mm-diameter cylindrical specimens impinging vertically on a rotating disc coated with the 180 mesh SiC abrasive. Specimens were gravity loaded with a mass of 320 g. Cylindrical samples were spark machined from the top layer of the weld deposits, so that the test surface was parallel to the layers of hardfacing alloy. A maximum course of 600 wheel revolutions (approximately 15 minutes) was adopted for all the tests. The rotating speed of the disc was fixed at

45 rpm, the length of the wear path was 64 mm, and the relative velocity of the disc with respect to the sample was 9 mm s^{-1} . At the end of each 200 wheel revolutions, the volume loss was determined and the abrasive paper was changed in order to avoid spurious effects due to the degradation of the abrasives during the wear tests.

III. RESULTS AND DISCUSSION

A. Solidification of Alloy 700

Primary Ti- and Nb-rich MC carbides are the first solid phase to become thermodynamically stable in the alloy, which precipitates massively from the liquid at ~ 2270 °C, as shown in Figure 1 from the Scheil simulation. The formation of these primary MC carbides probably begins from its heterogeneous nucleation on liquid impurities. The weight fraction of MC then increases gradually until the alloy reaches ~ 1866 °C. From this temperature, the formation of MC carbides enriched with W designated MC', together with more Ti and Nb-rich MC carbides, is predicted over a wide range of temperatures until the alloy reaches 1351 °C. Solidification proceeds with the massive precipitation of M_7C_3 between 1351 °C and ~ 1191 °C. Austenite becomes stable at ~ 1191 °C as 58 pct of liquid remains and few or none MC type carbides are expected to form

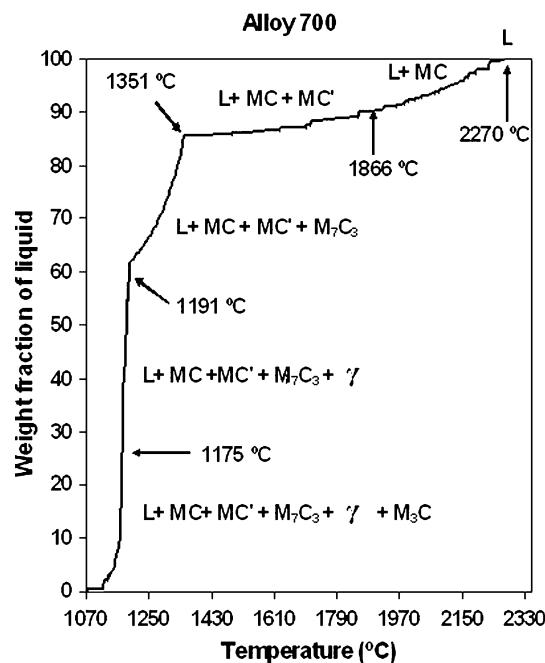


Fig. 1—Results of a Scheil simulation showing the solidification of alloy 700 under nonequilibrium conditions.

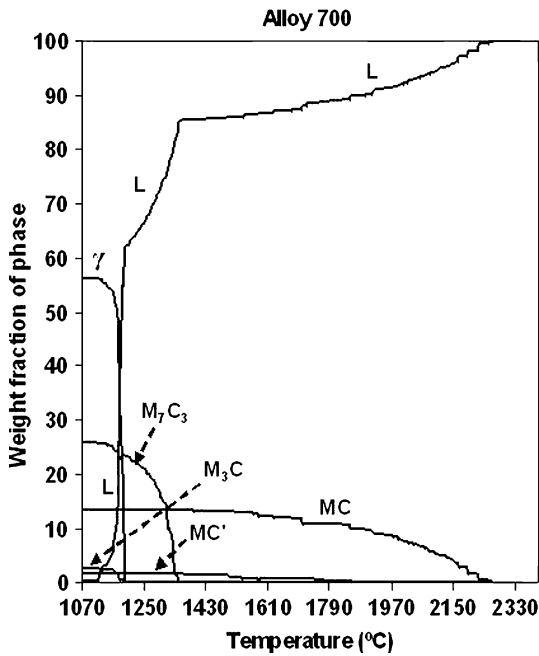
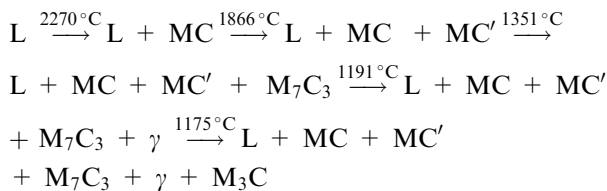


Fig. 2—Calculated weight fraction of phases in alloy 700 as a function of temperature.

below that temperature. The formation of M_3C is expected to begin at about 1175 °C until 1070 °C with the simultaneous formation of some M_7C_3 and more austenite. It is worthwhile mentioning that the formation of the M_3C carbides is not predicted in white iron containing 15 pct Cr and addition of 7 pct Nb, according to the liquidus projection proposed to Kesry *et al.*^[9]

Considering these results, the solidification of alloy 700 can be summarized as follows:



Thermodynamic calculations were also useful to calculate the theoretical volume fraction of the stable phases in alloy 700 in order to mark out results to be obtained from microstructural characterization. Figure 2 illustrates the proportion of these stable phases after complete solidification (no liquid remaining).

Figure 3 is the X-ray diffraction pattern of the hardfaced layer. Beside austenite and M_7C_3 peaks, there are also prominent peaks of NbC and TiC in the alloy 700. Those of TiC and NbC phases exactly overlap, and it is difficult to identify whether the carbides formed are (TiNb)C type carbides, rather than separated TiC and NbC carbides. Thus, the formed carbides need to be identified further by microstructural observation and microanalysis with SEM and energy-dispersive X-ray analysis (EDAX).

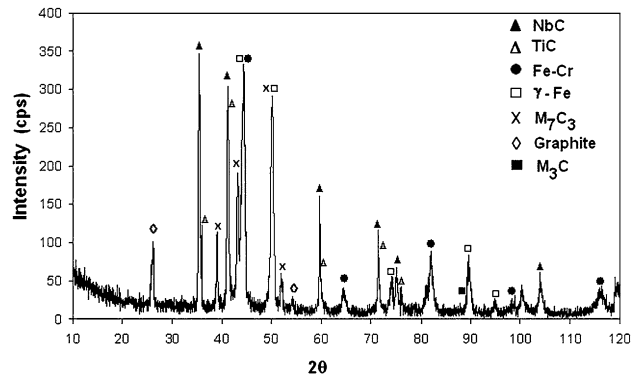


Fig. 3—X-ray diffraction pattern of alloy 700.

B. Microstructure

Even though W is a carbide forming element, from this X-ray diffraction pattern, the presence of WC could not be positively identified. This might be because the W present in the powder Fe-(TiW)C remained as stable $Ti_{0.5}W_{0.5}C$ carbide during the fusion, as might be expected. Furthermore, W is prone to partition into other carbides present such as NbC and M_7C_3 , rather than forming primary carbides. With relation to the phase M_3C , an X-ray peak is detected in $2\theta \cong 89$ deg, suggesting the presence of this phase.

Figures 4(a) and (b) are optical micrographs of the polished surface of the undiluted top layer of hardfacing alloy 700 and show a homogeneous distribution of small dendrites and finer spherulitic particles as well as the presence of large undiluted particles in the matrix (phase A). Microanalysis results (Table V) show that the large particles (phase A) are probably $Ti_{0.5}W_{0.5}C$ carbide reinforcements, which remained undiluted during fusion welding. These particles are similar to the powders from Fe-(TiW)C described in the literature.^[10] The Ti is mostly detected inside the particle, whereas W is mainly detected outside, indicating that the interior is mainly composed of TiC and the exterior is mostly composed of WC. It is worthwhile mentioning that a comparison between the calculated theoretical composition and the EDS results obtained for these particles suggests that phase A corresponds to the MC' carbides, as predicted in Figure 1.

Figure 5 is an optical micrograph of the alloy after etching. The most striking feature is the presence of large bright dendrites (phase B) in a eutectic matrix (phase M) besides the dendrites (phase C) and the fine spherulitic particles (phase D) already observed in Figures 4(a) and (b).

In order to investigate more carefully the possible presence of other fine phases, several observations of alloy 700 specimens in the as-welded condition were carried out using scanning electron microscopy. Back-scattered imaging revealed that phase C is enriched with one or more elements with high atomic number (*cf.* Figure 6), which was confirmed by EDS (Table VI). Phase C was found to be largely enriched in Ti and Nb

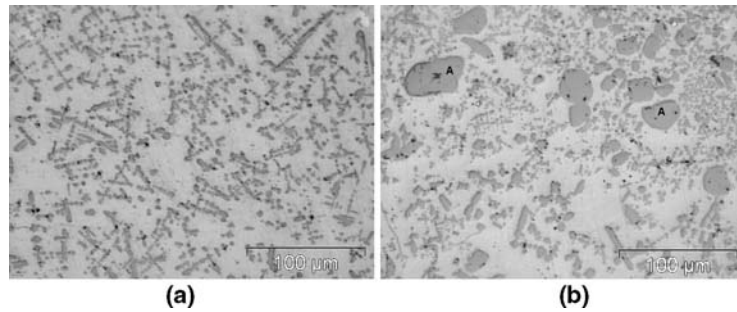


Fig. 4—Micrographs of the polished surface of alloy 700 showing (a) dendrites and fine spherulitic particles and (b) large particles labeled phase A.

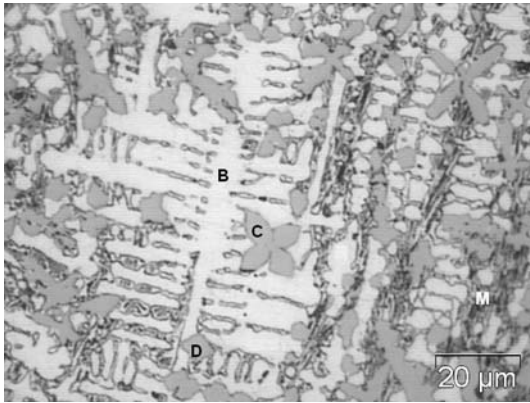


Fig. 5—Labeling of main phases present in alloy 700. B: large dendrites, C and D: randomly dispersed phases, and M: matrix, which appear mostly black.

Table V. Typical Chemical Composition Obtained by EDS Analysis for the Phase A, Ignoring the Carbon Content (Weight Percent)

Phase A	Particle Center	Particle Exterior
W	33.0	42.4
P	1.1	0.5
S	0.7	0.7
Ti	62.9	43.0
Cr	0.2	3.3
Fe	1.9	9.8

and is morphologically different; these results suggest that phase C is (TiNb)C. The EDS data shown in Table VI indicate that phase B is primary austenite dendrites with a high content of Cr. Microhardness measurements of this phase gave a value of 365 HV, which confirmed that phase B is primary austenite. The EDS microanalyses in two different points of the matrix (phase M) show that this is widely enriched in Cr and Fe (Table VI). These results and the morphology of the phase indicate that phase M is eutectic mixture γ/M_7C_3 .

Figure 7(a) is an SEM image of the fine spherulitic particles dispersed in the matrix (phase D), and Figures 7(b) through (f) are EDS mapping of Ti, Nb, W, Cr, and Fe inside the particle. The core area is probably a Ti-rich carbide, and its exterior is a W- and Nb-rich carbide. The area in which a significant amount of Fe is

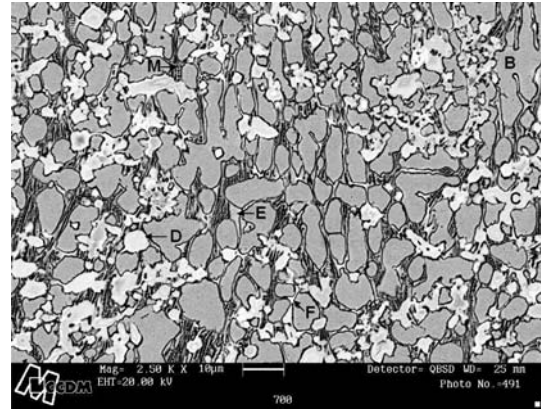


Fig. 6—Backscattered electron image of alloy 700 showing good contrast between phases and the presence of other finer phases.

detected, is an Fe matrix, which is reported to act as a binder.^[10] These spherulitic carbides present a similar pattern to the Fe-(TiW)C powders, except for the chemical composition. As with the FeWTiC powders, the interior and exterior of the spherulitic carbides are different, that is, the dark gray core areas mostly enriched with Ti are encircled by light gray areas. However, the main difference with Fe-(TiW)C is that the exterior light gray areas of spherulitic carbides were found to be mostly enriched of Nb rather than W. On the other hand, the W is homogeneously distributed mainly in the TiNbC carbides (phase C) and, to some extent, in the matrix. This is consistent with the earlier discussion.

Probably, during solidification, there was a replacement of a significant amount of W by Nb in the formation of spherulitic carbides, because Nb is a stronger carbide forming element than W and presents lower solubility in the liquid. The W, in turn, diffused itself to the liquid and, as the solidification proceeded, redistributed itself into the more stable phases already present in the liquid such as TiNbC carbides. Furthermore, the TiC stable core may have acted as the nucleus for the precipitating NbC and tied up some amount of Nb present in the liquid.^[3,11]

Figure 6 also revealed the presence of two fine phases labeled phases E and F. Microanalyses results (Table VI) showed that the chemical composition of

Table VI. Typical Chemical Composition of the Phases, Weight Percent

Phases	B	C	E	F	M Region Mostly Rich in γ	M Region Mostly Rich in M_7C_3
W	2.7	12.4	5.1	25.3	3.6	4.5
Nb	0.8	21.8	1.5	1.1	0.7	1.2
Ti	—	58.9	0.5	0.4	—	0.2
Cr	20.4	2.6	50.3	18.8	28.3	49.1
Fe	75.8	2.9	41.0	52.8	67.7	42.4
Ni	0.3	—	—	—	—	—

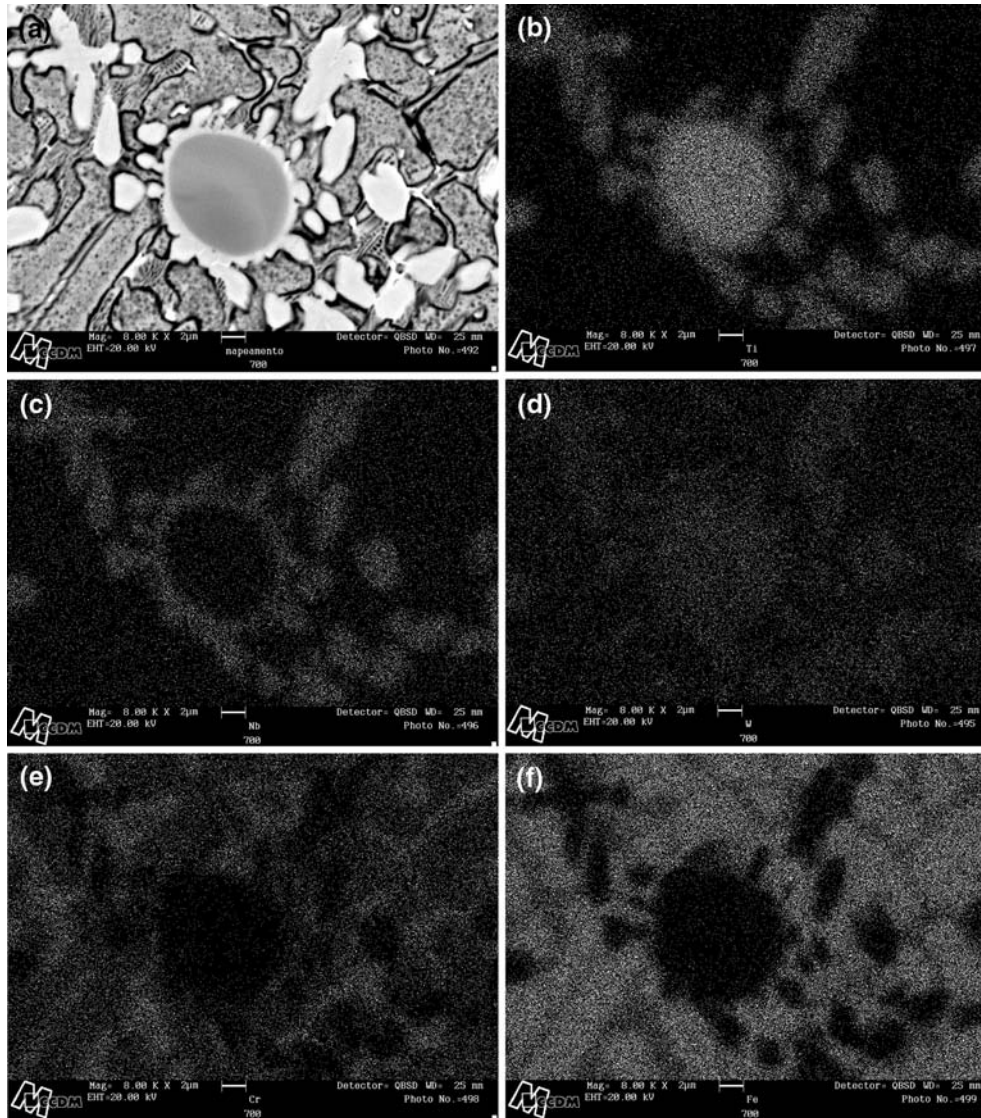


Fig. 7—(a) SEM image of phase D and (b) through (f) EDS mapping of Ti, Nb, W, Cr, and Fe of alloy 700 specimen.

phase E was found to be similar to phase M, except for the amount of W. Despite the limitation in resolution by EDAX, the chemical composition and the morphology of the phase suggest that phase E is fine primary M_7C_3 carbides. Chen *et al.*,^[12] studying the effect of Nb in white iron containing 15 pct Cr, concluded that Nb produces the refinement of primary M_7C_3 carbides. The EDS data (Table VI) also show that fine phase F

contained a high amount of Fe and W as well as ~19 pct Cr. Despite the fact that the solubility limit of Cr in M_3C phase is 15 pct according to the liquidus projection mentioned elsewhere in the literature,^[13,14] Berns *et al.*^[15] identified the presence of M_3C with Cr content ranging between 18 and 22 pct in white iron with additions of Nb, Ti, and B. Therefore, from the results obtained so far, together with information found in the

literature, it is reasonable to suggest that phase F is fine M_3C carbides.

Results obtained from image analysis to estimate the volume fraction of the phases present in alloy 700 are shown in Table VII. Chemical etching of the polished surface of metallographic specimens (Figures 4(a) and (b)) were used to obtain a good contrast for the fine particles. All of these particles presented the same contrast under light microscope, and EDS microanalyses showed that most of these are MC carbides. Heavy etching provided a good contrast between the phases M and B.

Area count results obtained with the computer programme "Analysis" are shown in Table VII. On the basis of the relationship between area and volume fractions, results shown in Table VII show that the

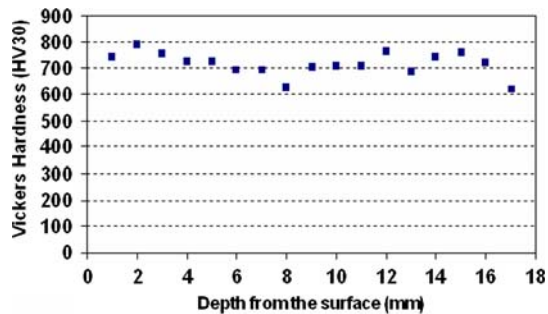


Fig. 8—Vickers hardness survey along the cross section of alloy 700.

average volume fraction of phases A, C, D, E, and F roughly composes 21 pct of the hardfacing material, which corresponds well to the theoretical volume fraction of the combined phases at 19 pct; it is reasonable to assume that the real volume fraction of each individual phase is well reflected, as shown in Figure 2.

C. Hardness and Wear Resistance

Figure 8 shows the Vickers hardness number measured along the depth from the surface of the hardfaced layer. The bulk hardness of the hardfaced layer remains fairly constant, regardless of the depth from the surface, and reaches an average hardness of 747 HV in the 5 mm upper part of the layer. Figures 9(a) and (b) provide the abrasion test results obtained for the alloy 700, the HCO, and the high-chromium white iron containing Nb. As can be seen in Figure 9(b), even though HCO and CNO present higher hardness (~793 HV and 763 HV, respectively), their high stress abrasion resistances are lower than alloy 700 (Figure 9(a)). This may be attributed to microcracking at the large hard and brittle primary M_7C_3 carbides present in both HCO and CNO and their subsequent removal from the matrix by spalling. Furthermore, the carbide fragments may behave as abrasive themselves, leading to a higher volume loss.^[16] Another wear mechanism present in these alloys is the pit formation along the carbide-matrix interface.^[17,18]

On the other hand, the better high stress abrasion resistance of alloy 700 may be attributed not only to the

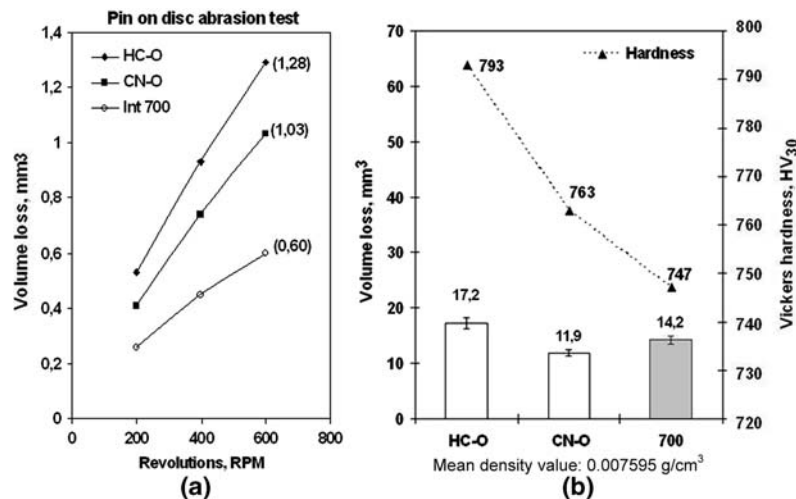


Fig. 9—Abrasion test results obtained during (a) high stress pin-on-disc test and (b) low stress RWAT test.

Table VII. Image Analysis Results of Alloy 700

Statistical Function	Phase M Eutectic γ/M_7C_3	Phase B Primary γ	Phase A + C + D + E + F
Unity	pct	pct	pct
Count	15	15	15
Mean	53.6	24.9	21.5
Standard deviation	0.8	3.9	1.3

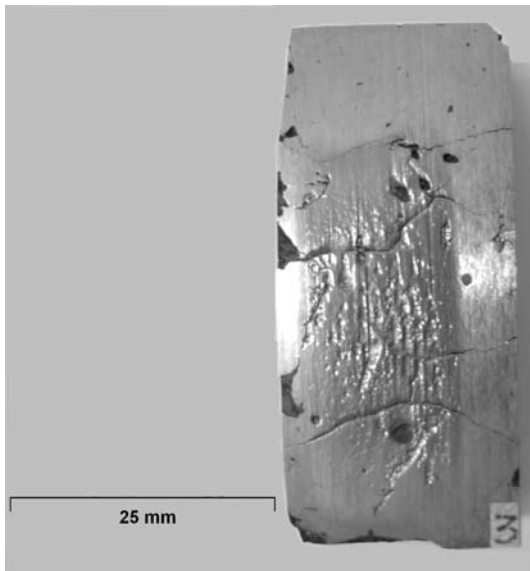


Fig. 10—Macrograph of low stress abrasion test specimen of alloy 700 showing the presence of porosity and lack of fusion.

higher carbide concentration but mainly to the presence of hard fine spherulitic carbides (TiNbW)C and, to some extent, of undiluted particles of (TiW)C complex carbide homogeneously dispersed in the eutectic matrix. It is suggested that these reinforcing particles firmly supported by the matrix minimized the effect of eventual deformation and spalling of the (TiNb)C carbide dendrites and avoided a severe abrasive wear of the matrix. Choo *et al.*,^[10] studying the effect of complex carbides in a hardfacing alloy, verified that the most important microstructural factor in determining the wear resistance of the hardfacing layer was the amount of these carbides. Furthermore, it was reported that the presence of a small amount of Nb in the matrix increases its strength.^[12] The presence of primary austenite dendrites (~25 pct) influenced favorably the wear resistance of the alloy providing higher toughness to the matrix and supporting the fine carbides.^[19]

It can be seen in Figure 9(b) that the low stress abrasion resistance of alloy 700 is not much higher than that of alloy HCO and is slightly lower than the CNO alloy despite its greater amount of carbide former. This finding may be attributed mainly to the higher amount of defects as porosity and lack of fusion in the wear specimen of the alloy 700 in comparison with the wear specimen of alloys HCO and CNO, when the open arc welding technique is used to deposit the layers. Probably, the porosities and lack of fusion present on the wear surface (Figure 10) facilitated the penetration of the sand particles into the matrix and, consequently, the removal of fine carbides, increasing the abrasive wear. Furthermore, the size of the sand particles (~200 μm) is supposed to contribute to an increase in the wear rate, because larger particles may penetrate more easily into the matrix containing austenite dendrites if the fine carbides are not close enough to avoid that.

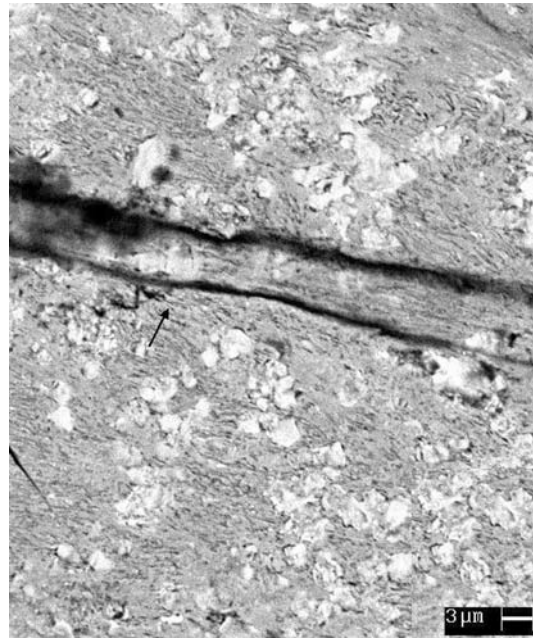


Fig. 11—Scanning electron micrographs of the worn surface of alloy 700 after pin-on-disc abrasion test using SiC (180 mesh) abrasives and a 320 g load. Note that the scratch groove width in reinforcement particles is seen to be narrower than in the matrix, suggesting that the reinforcement carbide particles improve the wear resistance.

However, it may be considered that the performance against the abrasive wear of alloy 700, with lower hardness and a tougher microstructure that is resistant to impact, was satisfactory in comparison with the conventional alloy HCO and CNO.

In order to understand the wear mechanisms present in alloy 700, Figure 11 shows an SEM micrograph of the worn surface after the pin-on-disc abrasion test using SiC abrasive paper. The observations suggest that reinforcement carbide particles are cut by the abrasive, but to a lesser extent than the matrix. Furthermore, the reinforcement carbide particles, apparently, protruded from the surface, and the scratch decreased in width as it crossed the region with the concentration of carbide particles.

IV. CONCLUSIONS

1. The present study showed that the addition of complex carbides composite powders as reinforcement in the eutectic matrix resulted in a microstructure with excellent wear abrasion resistance, mainly under high stress conditions.
2. Microstructural analyses suggest that spherulitic carbide particles presented a TiC carbide core encircled by a (NbW)C carbide, and there was a replacement of a large amount of W by Nb in the composition of the powder.
3. Microstructural observations also suggest that alloy 700 presents a tougher microstructure to enable impact resistance, without sacrificing the wear resistance.

ACKNOWLEDGMENTS

The authors are grateful to Welding Alloys Ltd. (UK) for providing welding consumables and equipment. The authors also thank Professor H.K.D.H Bhadeshia for the provision of the MTDATA program and the Brazilian Organization, CNPq.

REFERENCES

1. W.H. Jiang, W.D. Pan, G.H. Song, and X.L. Han: *J. Mater. Sci. Lett.*, 1998, vol. 17, pp. 1527–29.
2. C. Raghunath, M.S. Bhat, and P.K. Rohatgi: *Scripta Metall. Mater.*, 1995, vol. 32, p. 577.
3. W.H. Jiang, J. Fei, and X.L. Han: *Metall. Mater. Trans. A*, 2001, vol. 32A, pp. 431–33.
4. *User's Guide MT-DATA 4.70*, National Physical Laboratory, Teddington, United Kingdom.
5. M.J. Capaldi, A. Saidi, and J.V. Wood: *J. Mater. Synth. Processing*, 1996, vol. 4, pp. 245–53.
6. A. Saidi: *J. Mater. Processing Technol.*, 1999, vols. 89–90, pp. 141–44.
7. *Specifications for Carbides Products*, London and Scandinavian Metallurgical Co. Ltd., London.
8. *ASTM Standard G65-01*, ASTM, Philadelphia, PA, 2001.
9. R. Kesri and M. Durand-Charre: *J. Mater. Sci.*, 1987, vol. 22, pp. 2959–64.
10. S.H. Choo, C.K. Kim, K. Euh, S. Lee, J.Y. Jung, and S. Ahn: *Metall. Mater. Trans. A*, 2000, vol. 31A, pp. 3041–52.
11. F. Scandela and R. Scandela: *Mater. Sci. Technol.*, 2004, vol. 20, pp. 93–105.
12. H.X. Chen, Z.C. Chang, J.C. Lu, and H.T. Lin: *Wear*, 1993, vol. 166, pp. 197–201.
13. *Metals Handbook*, ASM, Metals Park, OH, 1983.
14. S. Atamert and H.K.D.H. Bhadeshia: *Mater. Sci. Eng. A*, 1988, vol. 130, pp. 101–11.
15. H. Berns and A. Fischer: *Metallography*, 1987, vol. 20, pp. 401–29.
16. H. Oh, S. Lee, J.Y. Jung, and S. Ahn: *Metall. Mater. Trans. A*, 2001, vol. 32A, pp. 515–24.
17. J.K. Fulcher, T.H. Kosel, and N.F. Fiore: *Wear*, 1983, vol. 84, pp. 313–25.
18. S.V. Prasad and T.H. Kosel: *Wear*, 1982, vol. 80, pp. 374–76.
19. J.D. Watson and P.J. Mutton: *Australian Welding Res.*, 1981, vol. 10, pp. 33–47.
20. R. Menon: *Weld. J.*, 2002, vol. 81, pp. 53–58.